Hindawi
Geofluids
Volume 2022, Article ID 9728261, 15 pages
https://doi.org/10.1155/2022/9728261

Research Article

Tripability Analysis of Casing Strings in Directional Wells Using the Continuous Beam-Column and Buckling Theory

Gang Wang, Gang Liu, Kai Wang, Yichen Li, and Yinan Hu

School of Petroleum Engineering, China University of Petroleum (East China), Qingdao 266580, China

Correspondence should be addressed to Gang Liu; lg_communication@126.com

Received 8 May 2022; Revised 27 June 2022; Accepted 12 July 2022; Published 30 July 2022

Academic Editor: Basim Abu-Jdayil

Hindered casing strings are often encountered in unconventional oil and gas exploration during the casing running process. This not only increases the operating costs and time but can also lead to downhole accidents and even abandonment in serious cases. Due to various assumptions, the calculation results of the existing soft models and hard models are different, which causes confusion for field operators when taking friction reduction measures. Moreover, a lowering force is often applied to assist hindered casing string running in a drilling field. However, its application is mainly based on work experience and lacks mechanistic analysis and theoretical guidance. Thus, in this study, a simulation model for the analysis of casing string tripability in a directional well was established and the model was combined with the continuous beam-column theory and buckling theory. The model was used to study how various factors including the friction coefficient, drilling fluid density, and casing diameter could affect the lowering force required when a casing string was hindered by buckling. The results showed that the maximum lowering force and the maximum effective lowering force decreased with the increase in the friction coefficient and the performance of the drilling fluid could be adjusted rapidly, which would be beneficial for ensuring that the casing string could be tripped smoothly by applying a lowering force. The increase in the drilling fluid density caused the maximum lowering force and the maximum effective lowering force to decrease, which was not conducive to hindered casing string running. The larger the casing diameter was, the greater the maximum lowering force and the maximum effective lowering force were. It was more convenient to apply a lowering force for a casing with a large diameter. In addition, the improved model could identify whether the casing string was in contact with the upper or lower borehole walls. Through finite element method verification, the prediction was in line with the actual casing running operation and the improved model has the smallest prediction error, i.e., 6.58%, compared with the existing models. Therefore, the improved model might provide necessary theoretical guidance for casing running operations in directional wells.

1. Introduction

Unconventional oil and gas exploration and development have entered an active period. Directional well technologies such as horizontal wells, extended reach wells, and cluster wells have been widely applied in unconventional oil and gas exploration. Casing strings cannot be tripped at the target depth due to the influence of the formation lithology, well trajectory, and casing running technology. Once the casing string running is hindered, it increases the operating cost and time and can lead to downhole accidents and even abandonment in serious cases [1]. Therefore, to ensure that the casing string reaches the target depth smoothly, it is necessary to predict the friction and applied lowering force.

At present, several models have been established for calculating the drag and torque of a tubular string. The soft-string torque and drag model was initially developed by Johancsik et al. [2] and later put in a standard differential form by Sheppard et al. [3]. This model assumed that the string was in continuous contact with the borehole wall and did not consider the string stiffness [4–7]. It is generally believed that the soft string model sometimes provides poor results for stiff tubular strings, high dogleg severity (small radius of curvature), or narrow radial clearance in the annulus [8].

Because the soft-string model does not consider the influence of the string stiffness, Ho. [9] established a stiff-string model for drag and torque based on the theory of large deformation for a drill string. Mitchell et al. [10] established a differential form that was easy to understand. However, many factors, including the variable stiffness of the tubular strings, the shape of the wellbore, and the clearance, can influence the contact state of the tubular strings and the value of the contact force on the tubular strings. The present stiff string models do not consider these factors, making it difficult to predict accurate results [11–13].

To improve the agreement between the calculation results and the real situation of a casing string running in a wellbore, 3D finite element models have been established to analyze the friction, stress, and deformation of the string in the build-up section and the horizontal section during the tubular string running process [14–20]. The well depth is generally several thousand meters. With the increase of the size of the 3D model, it is necessary to take a long time to complete calculations. The results are difficult to apply in real time in the field; it is often used to provide a reference for the optimal design of the wellbore trajectory and tubular string assembly and verify the accuracy of the new model for prediction drag and torque [21].

The continuous beam-column theory has been increasingly recognized because of its clear physical meaning and relatively simple algorithm [22–24]. When calculating the contact force between the string and the borehole wall in the traditional continuous beam-column theory, the contact point between the string and the borehole wall is first specified but one must generally be very cautious when specifying the contact point. As a result, some real contact points are missed, and in order to find these contact points, it is necessary to judge whether the deflection of the string between the two contact points exceeds the wellbore clearance. However, the traditional model does not consider the effect of a curved borehole on the deflection of the casing string, which cannot be ignored in the curved section.

Therefore, to identify the contact point between the pipe string and the well wall and ensure that the casing string runs smoothly in the directional well, the influence of the initial bending of the casing string on the deflection and deformation of the casing string was considered in this study using the improved continuous beam-column model. In addition, based on buckling theory, a prediction model of the maximum effective lowering force required during hindered casing string running was established. Using the existing friction model for tubular strings and field data verification, the model prediction results were proven to match the actual field data well.

2. Casing String Tripability Analysis Model

A model was established to predict whether a casing string could be run smoothly during the casing running process in a directional well. The primary reason that casing strings cannot be tripped in is the friction force. When the total friction of casing strings is greater than the floating weight of the casing strings above the stuck point, the casing strings are hindered during the casing running process. The friction force is generated by the contact between the casing strings and the wellbore wall. Therefore, the contact force is required to be analyzed first.

2.1. Basic Assumptions

(a) The string, which was composed of a casing, coupling, and centralizer, was regarded as an elastic beam column, and its deformation was within the linear elastic range

(b) The wellbore had a uniform circular cross-section without enlargement or hole shrinkage

(c) The coupling, centralizers, and other parts with relatively large diameters on the string or specified points of a certain length were taken as supports that were in contact with the borehole wall

(d) The casing string rotation and vibration were neglected

2.2. Three-Dimensional Wellbore Trajectory Plane Decomposition. The three-dimensional wellbore could be approximately represented in two dimensions by decomposing it into two planes, plane P and plane Q [25], as shown in Figure 1. The lateral force and deflection of the string were calculated on the two planes separately. Then, the lateral force and deflection of the string in space could be obtained after the corresponding superposition.

2.3. Establishing a Bottom-Hole Coordinate System. Based on the unit vector of the three coordinate axes in the bottom-hole coordinate system [26], the coordinate transformation matrix $[M]$ of the vector from the wellhead coordinate system to the bottom-hole coordinate system could be obtained as follows:

$$[M] = \begin{bmatrix} \cos a_b \cos \phi_b & \cos a_b \sin \phi_b & -\sin a_b \\ -\sin \phi_b & \cos \phi_b & 0 \\ -\sin a_b \cos \phi_b & -\sin a_b \sin \phi_b & -\cos a_b \end{bmatrix}, \quad (1)$$

where a_b and ϕ_b are the well inclination and the azimuth at the casing shoe, respectively. The coordinate transformation was as follows:

$$\begin{Bmatrix} x \\ y \\ z \end{Bmatrix} = [M] \cdot \begin{Bmatrix} N - N_b \\ E - E_b \\ H - H_b \end{Bmatrix}, \quad (2)$$

where H_b, N_b, and E_b are the H, N, and E coordinates of the casing shoe, respectively. H, N, and E are the coordinates of any point in the wellhead coordinate system, and x, y, and z are the x, y, and z coordinates of the corresponding points in the bottom-hole coordinate system, respectively.

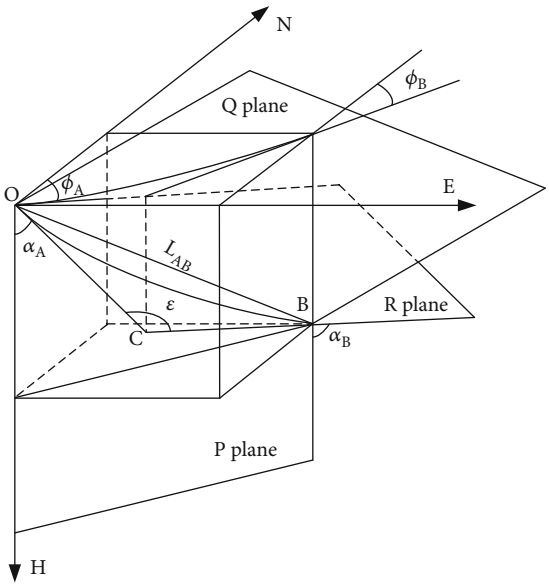

Figure 1: Three-dimensional plane decomposition of borehole trajectory.

2.4. Continuous Beam-Column Model

2.4.1. Three-Moment Equations in Plane P. With the casing string runs in plane P (well inclination plane) as an example, the casing string combination of any number (n) of centralizers was taken as the analysis object. As shown in Figure 2, the centralizers divided the whole casing string into N span beams and the transverse load q_i, bending moments M_{i-1} and M_i, and the axial force F_i acted on the ith span beam. The right deflection angle of the ith span beam was θ_i^R, the shear force was Q_i^R, the transverse load was q_{i+1}, the bending moments were M_i and M_{i+1}, and the axial force F_{i+1} acted on the $(i+1)$th span beam. The right rotation angle of the $(i+1)$th span beam was θ_{i+1}^L, and the shear force was Q_{i+1}^L.

The deflection curves of the two adjacent spans had a common tangent line at the support of the string. Therefore, the rotation angles on both sides of the support were equal:

$$\theta_{i,P}^R = -\theta_{i+1,P}^L. \tag{3}$$

The rotation angle at the support could be obtained from the formula of the end rotation angle and the deformation superposition principle of continuous beam-column theory (Appendix A):

$$\begin{aligned}
\theta_{i,P}^R &= \frac{q_{i,P}L_i^3}{24EI_i}X(u_{i,P}) + \frac{M_{i,P}L_i}{3EI_i}Y(u_{i,P}) + \frac{M_{i-1,P}L_i}{6EI_i}Z(u_{i,P}),\\
\theta_{i+1,P}^L &= \frac{q_{i+1,P}L_{i+1}^3}{24EI_{i+1}}X(u_{i+1,P}) + \frac{M_{i+1,P}L_{i+1}}{3EI_{i+1}}Y(u_{i+1,P}) + \frac{M_{i+1,P}L_{i+1}}{6EI_{i+1}}Z(u_{i+1,P}),\\
\theta_{n+1,P}^R &= \frac{q_{n+1,P}L_{n+1}^3}{24EI_{n+1}}X(u_{n+1,P}) + \frac{M_{n+1,P}L_{n+1}}{3EI_{n+1}}Y(u_{n+1,P}) + \frac{M_{n+1,P}L_{n+1}}{6EI_{n+1}}Z(u_{n+1,P}),
\end{aligned} \tag{4}$$

where L_i is the length of the ith span beam (m), $q_{i,p}$ is the component of the transverse load of the ith span beam in the P plane (N), a_i is the well inclination angle at the ith support (°), w_i is the weight per meter of the ith span beam in mud (kg/m), F_i is the average axial force on the ith span beam (N), E is the elastic modulus of the string (Pa), and I_i is the section moment of inertia of the ith span beam (m^4).

2.4.2. Initial Rotation Angle. For the actual string combination, the diameter of the centralizer was smaller than the diameter of the borehole. Therefore, when the string was tripped in the borehole, the centralizer might have been close to a side of the wellbore wall, which would have caused the displacement of the support due to the elimination of clearance. Therefore, several supports were not in a straight line. This resulted in an additional rotation angle at the end of the beam column due to the displacement of the supports, as shown in Figure 3.

In plane P, the initial additional rotation angle generated by the initial relative displacement of the supports at both ends of the ith span beam was

$$\delta\theta_{i,P}^0 = \arctan\left(\frac{\delta x_i^0 - \delta x_{i-1}^0}{z_i - z_{i-1}}\right). \tag{5}$$

In plane Q, the initial additional rotation angle generated by the initial relative displacement of the supports at both ends of the ith span beam was

$$\delta\theta_{i,Q}^0 = \arctan\left(\frac{\delta y_i^0 - \delta y_{i-1}^0}{z_i - z_{i-1}}\right). \tag{6}$$

2.4.3. Three-Moment Equations. Considering the initial additional rotation angle generated by the displacement of the support, the corresponding three-moment equation of the $(n+1)$th span continuous beam-column in the plane P could be obtained:

$$\begin{aligned}
&M_{i-1,P}\frac{L_iZ(u_{i,P})}{6EI_i} + M_{i,P}\left[\frac{L_iY(u_{i,P})}{3EI_i} + \frac{L_{i+1}Y(u_{i+1,P})}{3EI_{i+1}}\right]\\
&\quad + M_{i+1,P}\frac{L_{i+1}Z(u_{i+1,P})}{6EI_{i+1}} = -\frac{q_{i,P}L_i^3X(u_{i,P})}{24EI_i}\\
&\quad - \frac{q_{i+1,P}L_{i+1}^3X(u_{i+1,P})}{24EI_{i+1}} + \delta\theta_{i+1,P}^0 - \delta\theta_{i,P}^0,\\
&\frac{q_{n+1,P}X(u_{n+1,P})L_{n+1}^3}{24EI_{n+1}} + M_{n+1,P}\frac{Y(u_{n+1,P})L_{n+1}}{3EI_{n+1}}\\
&\quad + M_{n,P}\frac{Z(u_{n+1,P})}{6EI_{n+1}}L_{n+1} = \theta_{n+1,P}^R - \delta\theta_{n,P}^0.
\end{aligned} \tag{7}$$

The boundary conditions at the casing shoe and the upper tangent point in plane P were

$$\begin{aligned}
M_{0,P} &= 0,\\
M_{n,P} &= E\cdot I_n\cdot k_{aT},
\end{aligned} \tag{8}$$

where k_{aT} is the rate of well inclination change at the tangent point.

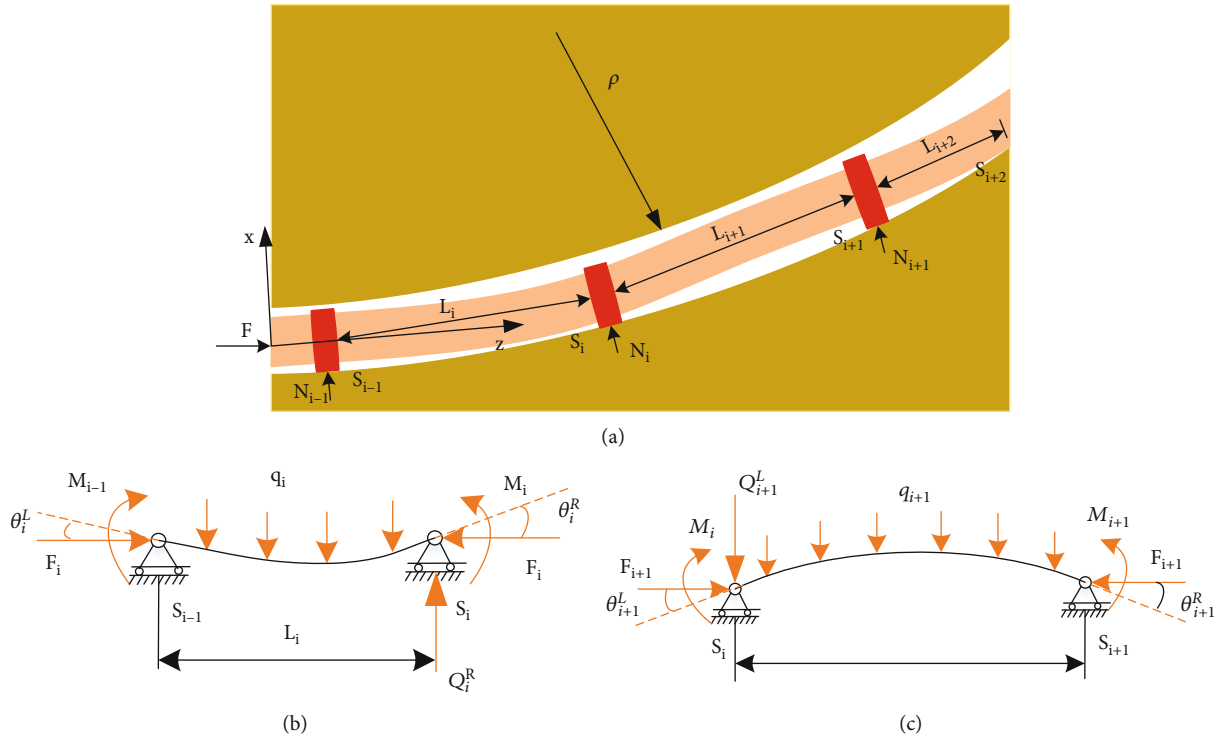

Figure 2: Force and deformation of casing string running in a curved section. (a) Schematic diagram of casing string running in a curved section. (b) Force and deformation of the ith span beam. (c) Force and deformation of the $(i+1)$th span beam.

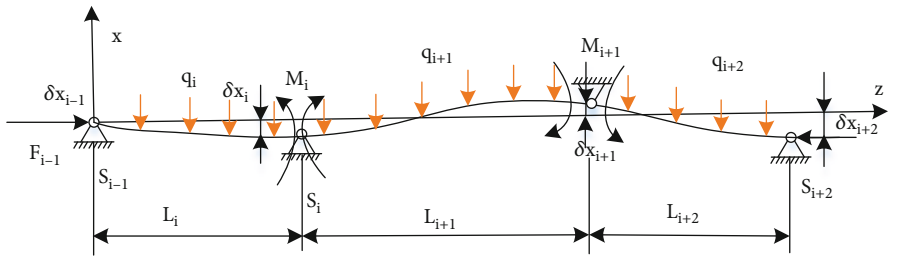

Figure 3: Schematic diagram of beam supports not in a straight line under the combined force.

There were $n+1$ equations for the three bending moments, in which the $n+1$ unknowns were $M_1 \sim M_n$ and L_{n+1}. Thus, there was a definite solution. For the ith beam support in plane Q, the left and right sides were the ith and $(i+1)$th span beams, respectively. Based on the continuous condition that the rotation angle of the beams on both sides of the support were equal, the three bending moment equations in plane Q were obtained.

$$M_{i-1,Q}\frac{L_i Z(u_{i,Q})}{6EI_i} + M_{i,Q}\left[\frac{L_i Y(u_{i,Q})}{3EI_i} + \frac{L_{i+1} Y(u_{i+1,Q})}{3EI_{i+1}}\right] + M_{i+1,Q}\frac{L_{i+1} Z(u_{i+1,Q})}{6EI_{i+1}} = \delta\theta^0_{i+1,Q} - \delta\theta^0_{i,Q},$$

$$M_{n+1,Q}\frac{Y(u_{n+1,Q})L_{n+1}}{3EI_{n+1}} + M_{n,Q}\frac{Z(u_{n+1,Q})}{6EI_{n+1}}L_{n+1} = \theta^R_{n+1,Q} - \delta\theta^0_{n,Q}, \quad (9)$$

Table 1: Critical load for the helical buckling of the string in different well sections, where F_{hel} is the critical load of helical buckling (N), r is the borehole annulus clearance (m), and R is the string radius (m).

Well section	Critical load for helical buckling
Vertical	$F_{hel} = 5.55\sqrt[3]{EIw^2}$
Straight inclined	$F_{hel} = 2.83\sqrt{EIw \sin a/r}$
Curved	$F_{hel} = 12EI/rR\left[1 + \sqrt{(1 + rR^2 w \sin a/8EI)}\right]$
Horizontal	$F_{hel} = 2\left(2\sqrt{2} - 1\right)\sqrt{EIw/r}$

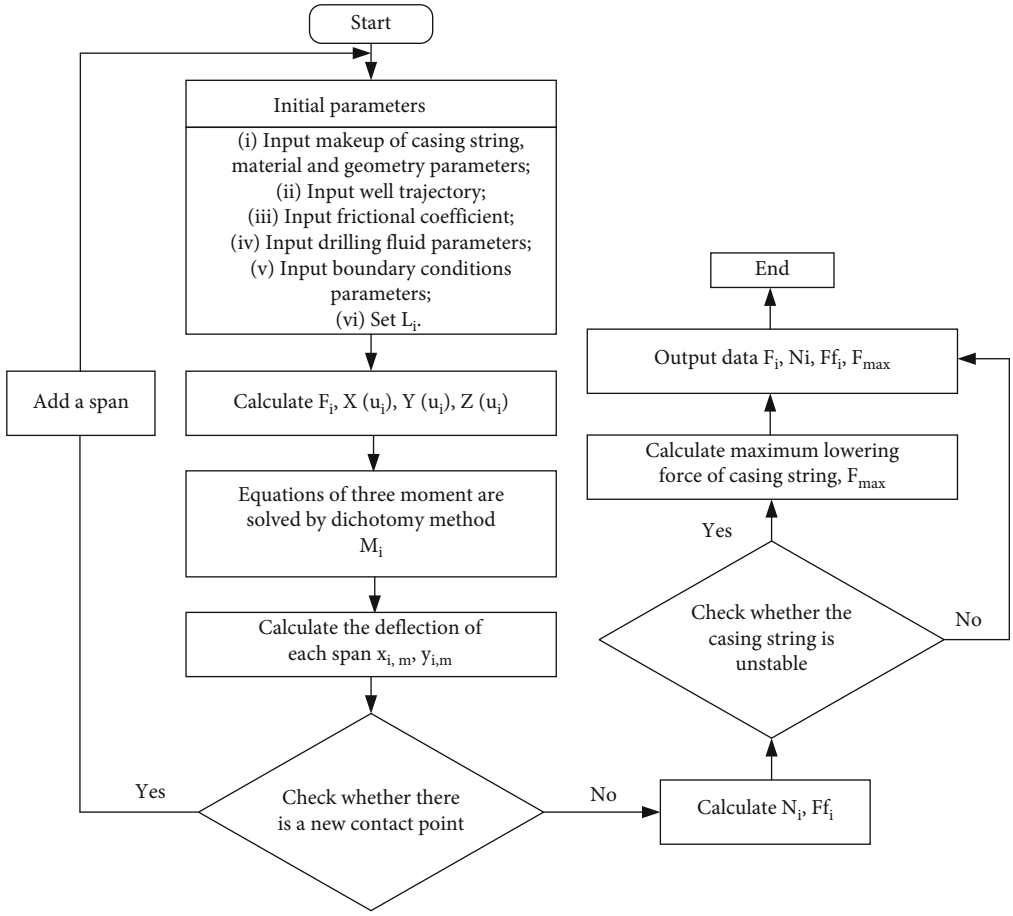

Figure 4: Flowchart of the solution procedure.

where the meanings of the parameters are the same as those above discussed.The boundary conditions at the casing shoe and the upper tangent point in plane Q were as follows:

$$\begin{aligned} M_{0,Q} &= 0, \\ M_{n,Q} &= E \cdot I_n \cdot k_{\phi T} \sin a_T, \end{aligned} \tag{10}$$

where $k_{\phi T}$ is the rate of azimuth change at the tangent point and a_T is the well inclination at the tangent point.

2.4.4. Contact Force. The relationship between the force and deformation of the string is given. An iterative method could be used to solve the deflection function of each span to obtain the deflection, rotation angle, and bending moment of the string after deformation. Combined with Figures 2(b) and 2(c), the contact force at each support in plane P could be calculated:

$$N_{i,P} = \frac{M_{i-1,P} - M_{i,P}}{L_i} + \frac{q_{i,p}L_i}{2} + \frac{M_{i+1,P} - M_{i,P}}{L_{i+1}} + \frac{q_{i+1,p}L_{i+1}}{2}, \quad (i = 1 \text{ to } n-1). \tag{11}$$

Then, the contact force at each support in plane Q was

$$N_{i,Q} = \frac{M_{i-1,Q} - M_{i,Q}}{L_i} + \frac{M_{i+1,Q} - M_{i,Q}}{L_{i+1}}, \quad (i = 1 \text{ to } n-1). \tag{12}$$

2.5. Effect of Initial Bending on Casing Deflection. When the casing string was tripped in the curved section of a wellbore, the deformation of the entire casing string had to be generally consistent with the wellbore axis. Therefore, the maximum deflection of the casing string caused by the initial bending could be obtained [27] (Appendix B):

$$x_{i,\max} = x_{i,0} + x_{i,1} = \frac{2\zeta_{i,P}}{u_i^2}\left(\frac{1}{\cos u_i} - 1\right) = \frac{K_{i,P}EI_i}{F_i}\left(\frac{1}{\cos u_i} - 1\right). \tag{13}$$

2.6. Judgment of Contact Points. Considering the influence of the borehole bending on the casing string deformation, the improved maximum deflection $x_{i,m}$ in plane P and the

improved maximum deflection $y_{i,m}$ in plane Q of the ith span string were calculated as follows:

$$x_{i,m} = \frac{q_{i,p}\Delta L_i^4}{16EI_i u_i^4}\left(\frac{1}{\cos u_i} - 1 - \frac{u_i^2}{2}\right) + \frac{M_{i-1,p} + M_{i,p}}{2F_i \cos(\Delta\alpha_i/2)}\left(1 - \frac{1}{\cos u_i}\right) + \frac{K_P L_i^2}{4u_i^2}\left(\frac{1}{\cos u_i} - 1\right) + \frac{e_{i-1,P} + e_{i,P}}{2},$$

$$y_{i,m} = \frac{M_{i-1,Q} + M_{i,Q}}{2F_i \cos(\Delta\phi_i/2)}\left(1 - \frac{1}{\cos u_i}\right) + \frac{K_Q L_i^2}{4u_i^2}\left(\frac{1}{\cos u_i} - 1\right) + \frac{e_{i-1,Q} + e_{i,Q}}{2}. \quad (14)$$

Therefore, the criterion for generating the new contact points was

$$\sqrt{x_{i,m}^2 + y_{i,m}^2} > \frac{D_w - D_{0i}}{2}, \quad (15)$$

where K_Q is the curvature on the azimuth plane of the well section where the string is located (°/30 m), D_w is the borehole diameter (m), D_{ci} is the centralizer diameter (m), D_{0i} is the casing diameter (m), $e_{i-1} = (D_w - D_{ci-1})/2$, and $e_i = (D_w - D_{ci})/2$.Once the maximum deflection of the casing string between the two supports exceeded the wellbore clearance, there was a new contact point and new support needed to be added to perform the recalculation.

2.7. Tripability Judgment of the Casing String. The contact force and the friction at each contact point could be obtained as follows:

$$N_i = \sqrt{N_{i,p}^2 + N_{i,Q}^2}, \quad F_{fi} = \mu N_i, \quad (16)$$

where μ is the friction coefficient.When the total friction of the casing string was greater than the floating weight of the casing string above the stuck point, the casing string could be considered hindered during the casing running process:

$$\sum F_{fi} > w_i \cdot L_s, \quad (17)$$

where L_s is the length of the casing string above the stuck point (m).

At that time, it was difficult for the casing string to run with its own floating weight and it was possible to run the casing string with the help of the other processes. For example, a lowering force, a pick-up and release technique, and casing floating could be applied. Since the casing string buckled during the running process, it was also necessary to consider the case in which the casing string was hindered by buckling.

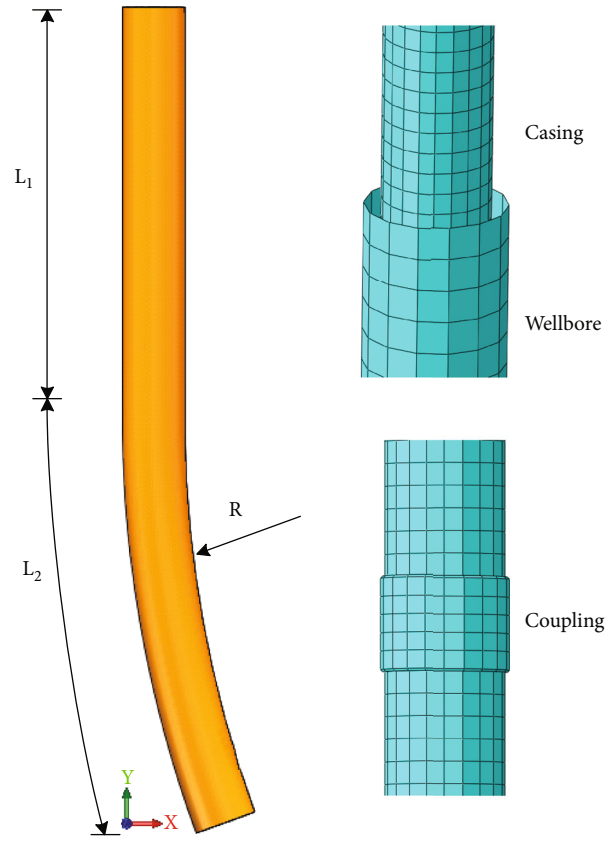

Figure 5: Finite element model of the casing string.

Table 2: Basic calculation parameters.

Name	Value
Well depth	4558 m
Kickoff point	1267 m
Build-up rate	4°/30 m
Radius of curvature, R	430 m
Vertical section, L_1	100 m
Build-up section, L_2	100 m
Diameter (borehole), D_w	215.9 mm
Diameter (casing), D_p	177.8 mm
Diameter (coupling), D_c	200.03 mm
Wall thickness (coupling), D_o	11.12 mm
Young's modulus, E	2.1×10^5 MPa
Poisson's ratio, ε	0.3
Friction coefficient	0.2

2.8. Critical Load for Helical Buckling of the String. Many scholars have obtained the critical load when a string is subjected to spiral buckling in different well sections through theoretical derivations or experiments, as shown in Table 1. Additional friction should be considered when a casing string is spirally buckling and in contact with a

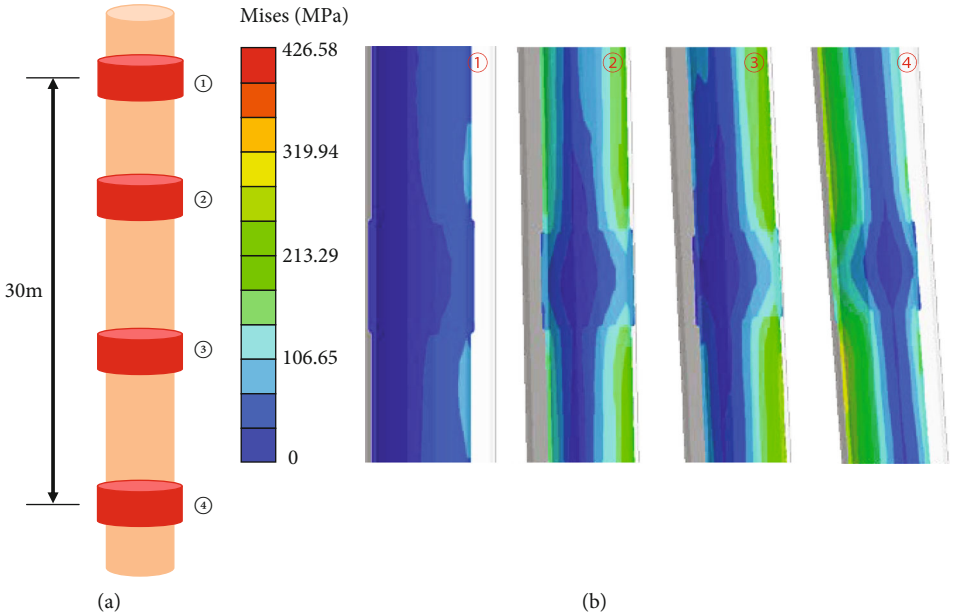

Figure 6: (a) Schematic diagram of casing string combination. (b) Cloud map of contact between the casing string and the wellbore wall.

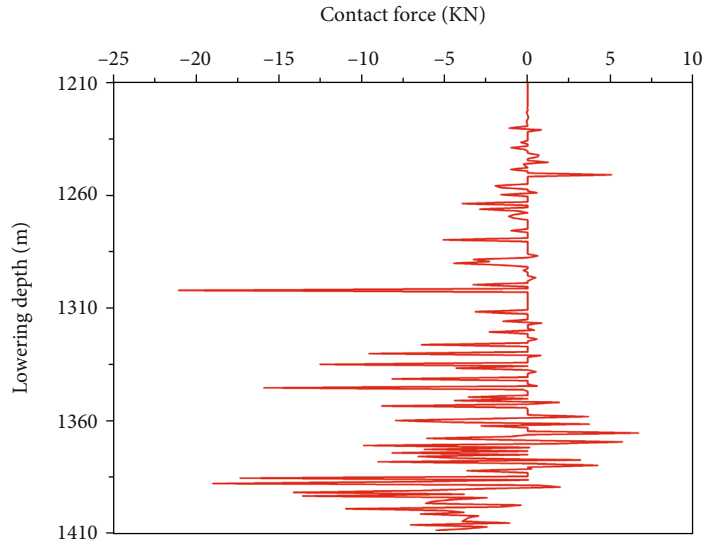

Figure 7: Contact force when the casing string was running in the wellbore.

borehole wall to determine whether the casing string can be successfully tripped in.

2.9. Determine the Maximum Lowering Force. Due to the restrictions of a wellbore, a string will undergo multiple deformation processes with the increase in the lowering force after string buckling. With the combined action of the string weight and the buoyancy of the drilling fluid, the string buckling becomes a spatial spiral shape with a varying pitch. The bending of the string causes contact with the borehole wall, resulting in increased friction, which offsets some of the lowering force and reduces the effective lowering force on the stuck point [28]. Therefore, how to determine the maximum lowering force when applying a load to push down the casing is very important for casing running.

The maximum lowering force $F_{\max}$ can be obtained as follows (Appendix C):

$$F_{\max} = \sqrt{\frac{w_m EI}{3\delta\mu r}}. \tag{18}$$

The maximum effective lowering force $F_{e\,\max}$ can be obtained as follows:

$$F_{e\,\max} = F_{\max} - \frac{\delta\mu r}{w_m EI} F_{\max}^3. \tag{19}$$

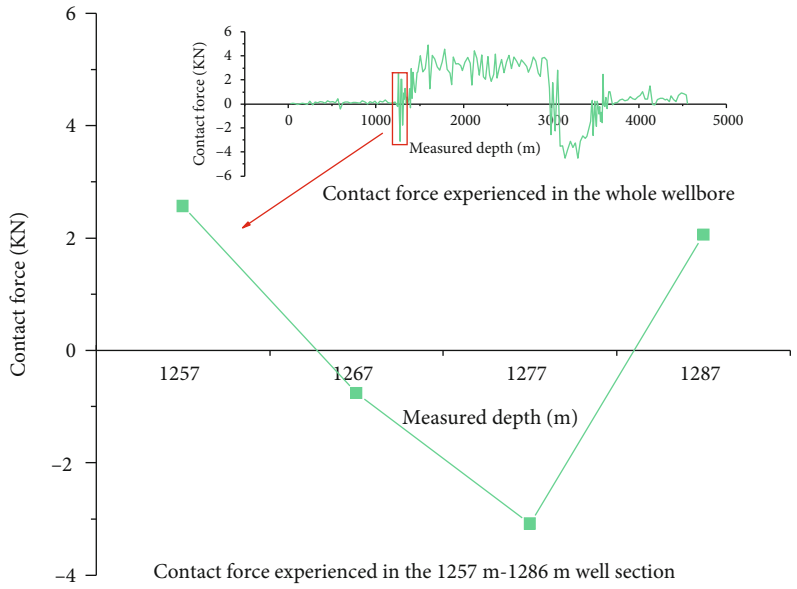

Figure 8: Contact force of the casing string using the improved model.

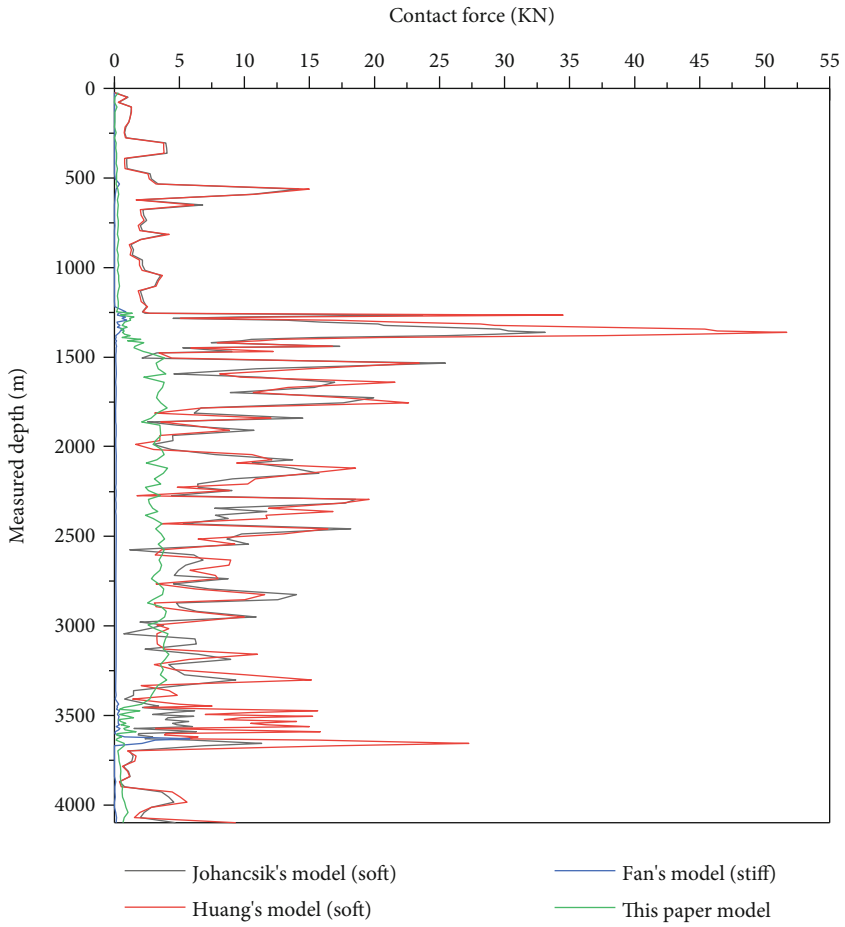

Figure 9: Contact force on the casing string using different models.

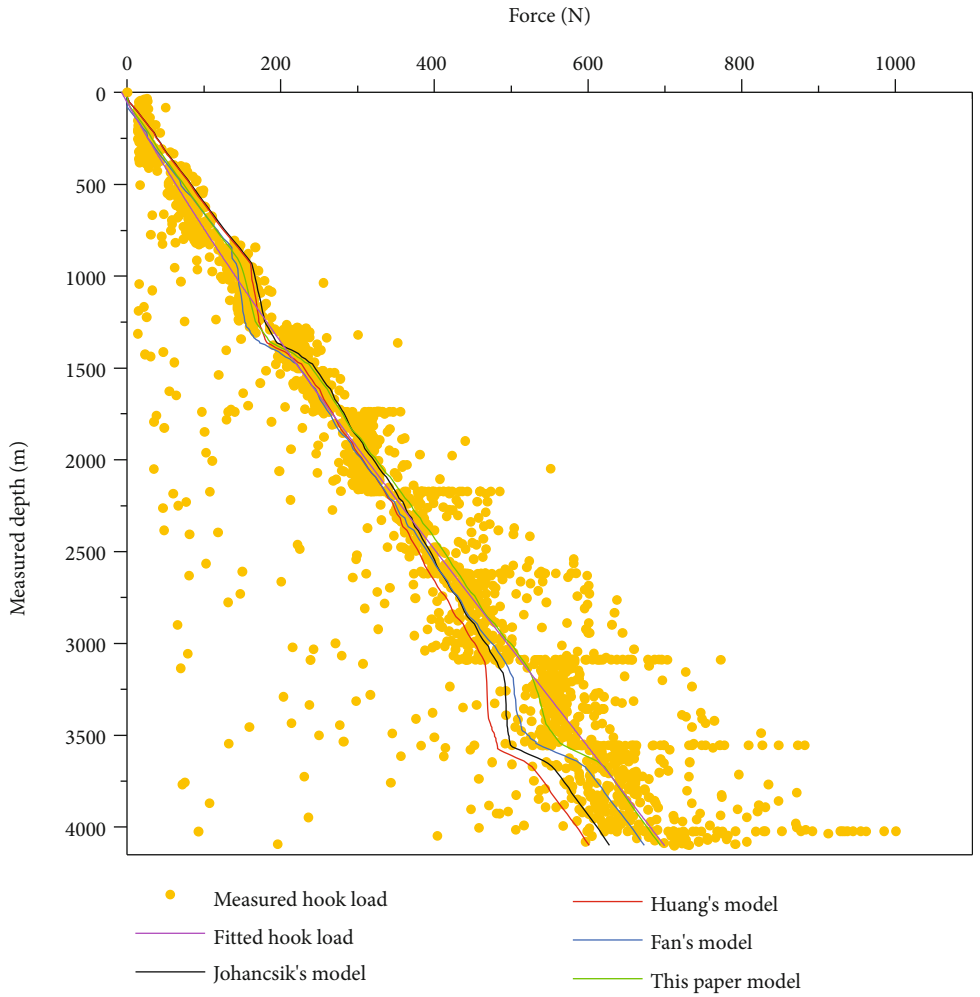

Figure 10: Axial load on the casing string using different models.

2.10. Solution Method. An iterative method [23, 24] was used to apply the simulation model in actual wellbores. The flowchart of the procedure is shown in Figure 4.

3. Model Validation

An example was adapted from an actual FX160 directional well in China. The finite element method was used for verification. Due to the large size of the actual borehole, the establishment of a full-size three-dimensional finite element model of the borehole trajectory and casing string combination required not only a high amount of computational resources but also a long time to perform the calculations. It was believed that the mechanical behavior of a point in the structure would have no effect on the point in space beyond 15 m [29]. Therefore, the well section at 1210–1410 m was selected. This section included the vertical section and the curved section. Considering the influence of the casing string coupling, the deformation and the contact force when the casing string was tripped in were simulated and calculated. The three-dimensional finite element model is shown in Figure 5. The relevant parameters in the model are shown in Table 2.

The dynamic explicit analysis method was used, and the casing running speed was 0.8 m/s. When the casing string was tripped in the wellbore, it deformed and came into contact with the borehole wall due to the influence of the curved borehole. Because the model size was large, the contact state of the entire casing string and the wellbore wall could not be clearly displayed. Therefore, only the contact cloud map of the casing string and the wellbore wall in the 1257–1287 m well section is illustrated in Figure 6. Figure 6(a) shows the schematic diagram of the casing string combination in this well section, and Figure 6(b) shows the corresponding cloud map of the contact between the 30 m casing string and the wellbore wall. As shown in Figure 6(b), the first and fourth couplings were in contact with the downhole wall and the second and third couplings were in contact with the upper wellbore wall. The simulation showed that due to the influence of the curved wellbore, the casing string occasionally came into contact with the upper or lower hole walls of the wellbore during the running process. The calculation results are illustrated in Figure 7. The magnitude and the direction of the contact force were constantly changing when the casing string was tripped in the 1210–1410 m well section.

Table 3: Comparison of model prediction errors.

Wellbore	Relative error (%)			
	Johancsik's model	Huang's model	Fan's model	This paper's model
	33.22	31.64	15.98	15.94
Vertical section	25.08	23.50	15.87	14.09
	13.81	10.56	−1.91	4.60
	17.10	9.01	−2.54	7.80
Build-up section	4.63	−1.92	−5.56	1.33
	9.20	2.70	0.03	7.34
	2.81	−1.70	−2.01	3.97
Sail section	−1.34	−5.16	−2.56	2.80
	−5.08	−8.38	−4.70	0.21
	−6.31	−9.40	−4.27	0.52
Drop-off section	−10.70	−15.04	−8.34	−2.72
	−16.18	−19.14	−10.58	−5.25
	−10.43	−14.64	−3.75	0.02
Inclined section	−10.43	−14.54	−3.83	−0.33
	−10.21	−14.18	−3.70	−0.61
Root mean square error (%)	14.36	14.52	7.41	6.58

The contact force when the casing string was tripped in the wellbore using the improved continuous beam-column model is shown in Figure 8. The casing strings are in contact with the upper or lower borehole wall in the curved section, resulting in changes in the direction and magnitude of the contact force. For the casing strings at 1257–1287 m, the direction of the contact force also changed, similar to the results in Figure 6(b).

The comparison of the results in Figures 7 and 8 showed that the magnitude of the contact force using the improved continuous beam-column model was different from that of the finite element simulation. The magnitude of the contact force calculated using the improved continuous beam-column model represented the contact force of each contact point between the casing string and the borehole wall, while the result of the finite element method was the resultant force of all contact points between the entire casing string and the borehole wall at a certain time. Although the contact force values calculated with the two methods were different, the direction of the contact force reflected the contact state between the casing strings and the wellbore wall when casing strings were tripped in the wellbore, which was more consistent with the actual running operation of the casing strings.

4. Field Applications

With the wellbore trajectory in Section 3 taken as an example, the established tripability analysis model of the casing string was used to calculate the contact force, hook load, and maximum lowering force required during the casing running in the wellbore. The proposed model was compared with the existing friction model of the string and the field drilling data.

Table 4: Casing string combination parameters.

Name	Value
Casing diameter	0.1778 m
Wall thickness	0.0115 m
Unit weight	466.676 N/m
Moment of inertia	2.09×10^{-5} m^4
Borehole diameter	0.2159 m
Young's modulus, E	2.1×10^{11} Pa

4.1. Contact Force on the Casing String. Figure 9 shows that the contact force calculated with the soft model was significantly greater than that of the stiff model. The reason for this was that the soft model assumed that the casing string was in continuous contact with the borehole wall, while the stiff model assumed point contact with the borehole wall. However, the contact force calculated based on the improved continuous beam-column model was also greater than that of Fan's model. The reason for this was that the new model considered the influence of the curved wellbore on the deformation of the casing string. When the string made new contact with the borehole wall due to the initial bending deformation, the additional contact force was included in the total contact force.

4.2. Hook Load of Casing Running. When the casing string was tripped in, its axial load was mainly affected by the floating weight of the string and the friction between the string and the borehole wall. The hook loads calculated by the four models are shown in Figure 10. The hook load calculated by the soft model was less than that calculated by the stiff model in the bottom hole. The reason for this was that the friction calculated by the soft model was larger than that of the stiff

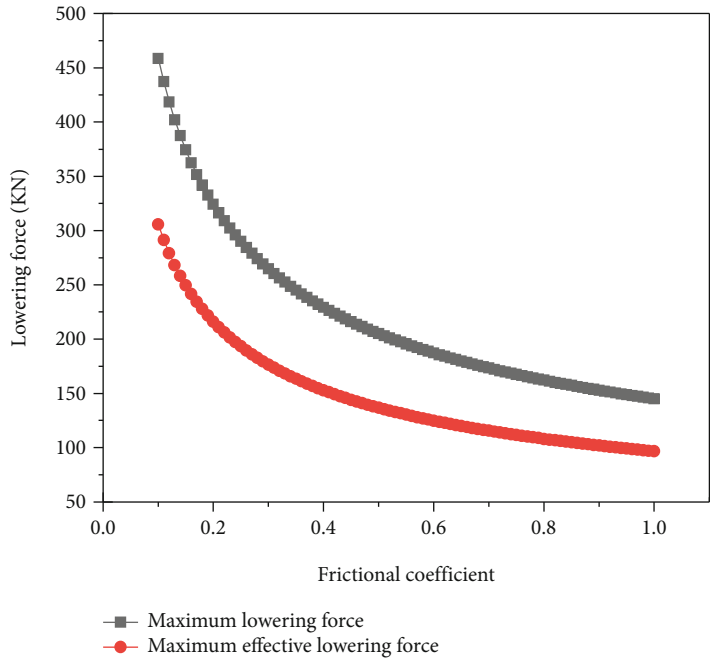

Figure 11: Lowering force on the casing string for different friction coefficients.

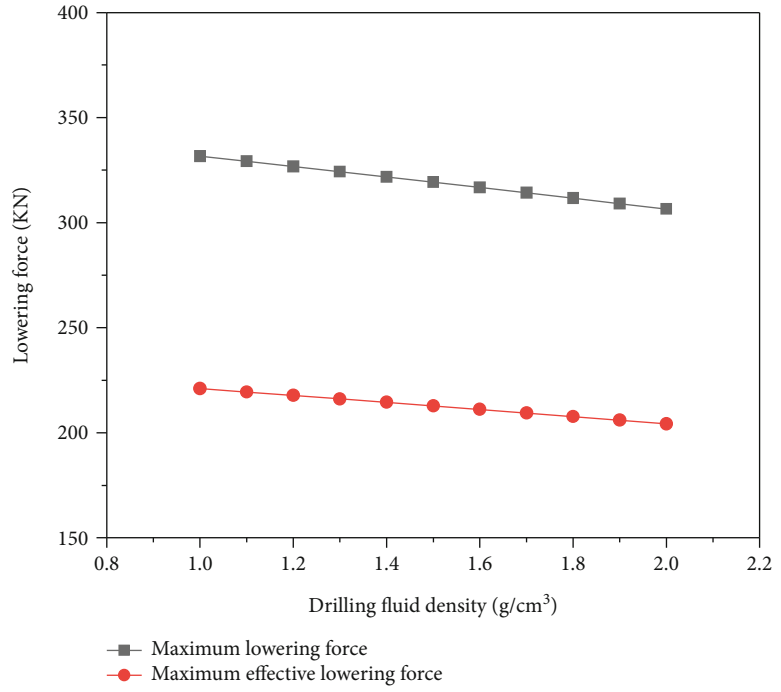

Figure 12: Lowering force on the casing string for different drilling fluid densities.

model and the friction direction was opposite to the movement direction of the casing string, which offset part of the floating weight of the casing string.

The measured hook load was highly affected and sensitive to any change in the drilling operation such as the drill string material gradient, outer diameter, inner diameter, bottom hole assembly, drilling fluid, drilling path, drilling trajectory, or dynamics of the hook. These made the measured hook load data points fluctuate greatly, which was inconvenient for the model verification. Therefore, the hook load data points were fitted with a polynomial function before validation and a fitting curve representing the hook load was obtained, as shown in Figure 10. The accuracies of the four models were verified by comparison with the

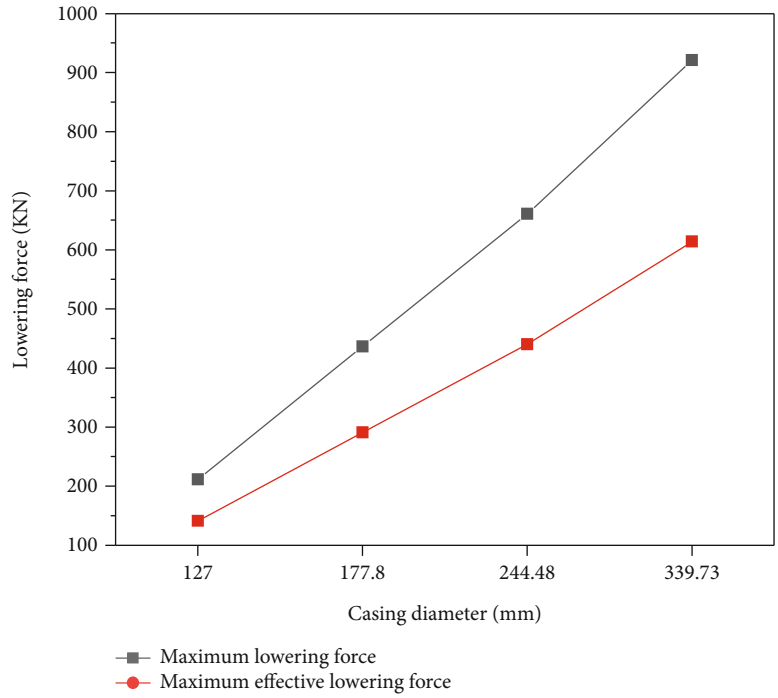

Figure 13: Lowering force on the casing string for different casing diameters.

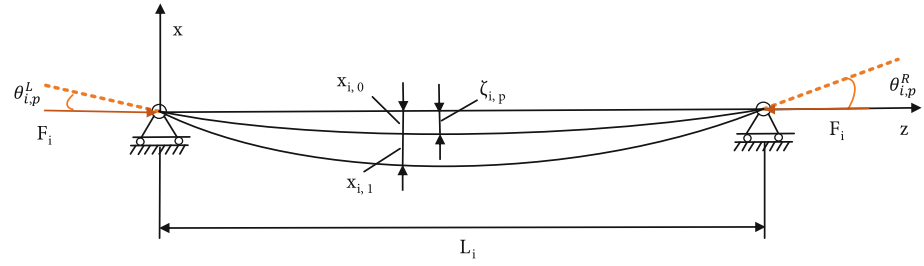

Figure 14: Beam-column with initial bending.

fitted curves. As shown in Table 3, 15 sets of large hook load data points were randomly selected from different well sections for comparison. It can be seen that the improved model had the smallest prediction error, i.e., 6.58%, compared with the existing models.

4.3. Maximum Lowering Force on the Casing String. With the 7-inch (177.8 mm) casing as an example, the parameters are shown in Table 4. The maximum lowering force and the maximum effective lowering force required for the buckled casing string to run in the wellbore were calculated.

Figure 11 shows that the maximum lowering force and the maximum effective lowering force decreased with the increase in the friction coefficient. Adjusting the performance of the drilling fluid at the appropriate time and reducing the friction coefficient increased the maximum lowering force and the maximum effective lowering force, which was conducive to applying a lowering force to the buckled casing during the casing running process.

As shown in Figure 12, the maximum lowering force and the maximum effective running force gradually decreased when the drilling fluid density increased from 1.0 to 2.0 g/cm^3, that is, increasing the drilling fluid density was not conducive to applying a lowering force to the buckled casing during the casing running process.

As shown in Figure 13, with the increase in the casing diameter, the maximum lowering force and the maximum effective lowering force increased and the difference between them also increased. The smaller the casing diameter was, the smaller the maximum lowering force and the maximum effective lowering force were. Therefore, the effect of applying the lowering force to the buckled casing with a smaller diameter was not as good as that for the buckled casing with a larger diameter.

5. Conclusions

(1) The casing string was hindered by buckling during the casing string running process. Improving the performance of the drilling fluid, reducing the friction coefficient, and reducing the drilling fluid density were conducive to applying a lowering force to the casing. The effect of applying the lowering force

to the casing with a smaller diameter was not as good as that for a casing with a larger diameter

(2) Compared with the existing models, the proposed model was no longer limited to the specified point contact range between the casing strings and the wellbore wall. Influenced by factors such as the well trajectory, string assembly, and drilling fluid performance, based on the specified point contact, newly added contact points were dynamically identified. The contact point might include contact with the upper or lower wellbore wall, which was close to the actual working conditions of casing strings running in the wellbore

(3) To account for the influence of the curved wellbore on the initial deformation of the casing strings, based on continuous beam-column theory and buckling theory, a comprehensive model for predicting the friction during casing string running and the lowering force required for hindered casing string running was established. A corresponding computer program was developed. Based on the field data verification, the improved model has the smallest prediction error, i.e., 6.58%, compared with the existing model. Therefore, the comprehensive model could be used for predicting the tripability of casing strings and the conclusions provided necessary theoretical guidance for casing running operations in directional wells

Appendix

A. Three-Moment Equations in Plane P

The rotation angle of the string at the upper tangent point is

$$\theta^R_{n+1,P} = \frac{\sum_{i=1}^{n+1} L_i}{\rho}. \tag{20}$$

The three-moment equations in plane P are

$$\begin{aligned}
\theta^R_{i,P} &= \frac{q_{i,P}L_i^3}{24EI_i}X(u_{i,P}) + \frac{M_{i,P}L_i}{3EI_i}Y(u_{i,P}) + \frac{M_{i-1,P}L_i}{6EI_i}Z(u_{i,P}),\\
\theta^L_{i+1,P} &= \frac{q_{i+1,P}L_{i+1}^3}{24EI_{i+1}}X(u_{i+1,P}) + \frac{M_{i+1,P}L_{i+1}}{3EI_{i+1}}Y(u_{i+1,P})\\
&\quad + \frac{M_{i+1,P}L_{i+1}}{6EI_{i+1}}Z(u_{i+1,P}),\\
\theta^R_{n+1,P} &= \frac{q_{n+1,P}L_{n+1}^3}{24EI_{n+1}}X(u_{n+1,P}) + \frac{M_{n+1,P}L_{n+1}}{3EI_{n+1}}Y(u_{n+1,P})\\
&\quad + \frac{M_{n+1,P}L_{n+1}}{6EI_{n+1}}Z(u_{n+1,P}),
\end{aligned} \tag{21}$$

where

$$\begin{aligned}
X(u_i) &= \frac{3}{u^3}(\tan u - u),\\
Y(u_i) &= \frac{3}{2u}\left(\frac{1}{2u} - \frac{1}{\tan 2u}\right),\\
Z(u_i) &= \frac{3}{2u}\left(\frac{1}{\sin 2u} - \frac{1}{2u}\right),\\
u_i &= \frac{L_i}{2}\sqrt{\frac{F_i}{EI_i}}w_i = w_{\text{pipe}}\left(1 - \frac{\rho_o}{\rho_{\text{pipe}}}\right),\\
q_{i,p} &= w_i \sin\left(\frac{a_{i-1}+a_i}{2}\right),\\
F_i &= -\sum_{j=1}^{i-1}\left[w_j\Delta L_j \cos\left(\frac{a_{j-1}+a_j}{2}\right)\right] - \frac{1}{2}w_i\Delta L_i \cos\left(\frac{a_{i-1}+a_i}{2}\right).
\end{aligned} \tag{22}$$

B. Effect of Initial Bending on Casing Deflection

The initial bending of the casing could be approximately considered to be consistent with the borehole curvature. If the deflection curve of the casing between the two centralizers was assumed to be a quadratic parabola, the approximate value of the maximum initial bending deflection was

$$\zeta_{i,P} = \frac{K_{i,P}L_i^2}{8}, \tag{23}$$

where $K_{i,P}$ is the borehole curvature when the ith span beam was located in plane P (°/30 m).With the action of axial and transverse forces, the initial bending of the casing string had a significant influence on the deformation of the casing string after being stressed. The most common method used to correct the effect of the initial bending is to replace the effect of the initial bending on the deflection with an equivalent transverse load and require the bending moment diagram of the transverse load to be the same as that of the axial force with initial bending. A schematic diagram of the string with initial bending is shown in Figure 14.

In Figure 14, $x_{i,0}$ is the initial bending deflection and $x_{i,1}$ is the bending deflection with the influence of the initial bending in Figure 14. It was assumed that the initial bending deflection curve was a quadratic parabola, namely,

$$x_{i,0} = \frac{4\zeta_{i,P}}{L_i^2}z_i(L_i - z_i), \tag{24}$$

where $\zeta_{i,P}$ is the maximum deflection of the initial bending and $M_{i,P} = F_{i,P}x_{i,0}$. The equivalent lateral load was

$$q_i = -\frac{d^2M_{i,p}}{dz_i^2} = -\frac{d^2(F_{i,P}x_{i,0})}{dz_i^2} = K_{i,P}F_i. \tag{25}$$

By substituting the lateral load into the bending deformation equation with the simultaneous action of a uniform load and an axial force, the maximum deflection of the casing string caused by the initial bending could be obtained:

$$x_{i,\max} = x_{i,0} + x_{i,1} = \frac{2\zeta_{i,P}}{u_i^2}\left(\frac{1}{\cos u_i} - 1\right) = \frac{K_{i,P}EI_i}{F_i}\left(\frac{1}{\cos u_i} - 1\right). \tag{26}$$

C. Determination of the Maximum Lowering Force

The contact force per unit length generated by the casing buckling on the borehole wall is

$$P = \delta \frac{rF^2}{EI}. \tag{27}$$

When the casing is bent in space, the total length of the deformed casing in contact with the borehole wall is

$$l = \frac{F}{w_m}. \tag{28}$$

The friction between the deformed casing and the borehole wall is

$$f = Pl\mu = \frac{\delta \mu r}{w_m EI} F^3. \tag{29}$$

The actual effective lowering force on the casing is

$$F_e = F - f = F - \frac{\delta \mu r}{w_m EI} F^3, \tag{30}$$

where F is the casing lowering force (N), F_e is the actual effective lowering force of the casing (N), and δ is a positive pressure coefficient.Part of the lowering force F applied on the casing is used to overcome the frictional force. It is not difficult to find that when the lowering force F increases, the effective lowering force F_e also increases. When the lowering force increases to a certain value, the effective lowering force has a maximum value. The derivative of the effective lowering force with respect to the lowering force is

$$\frac{dF_e}{dF} = 1 - \frac{3\delta \mu r}{w_m EI} F^2. \tag{31}$$

The maximum lowering force $F_{\max}$ can be obtained as follows:

$$F_{\max} = \sqrt{\frac{w_m EI}{3\delta \mu r}}. \tag{32}$$

The maximum effective lowering force $F_{e\max}$ can be obtained as follows:

$$F_{e\max} = F_{\max} - \frac{\delta \mu r}{w_m EI} F_{\max}^3. \tag{33}$$

Data Availability

The data used to support the findings of this study are available from the corresponding author upon request.

Conflicts of Interest

The authors declare that there are no conflicts of interest regarding the publication of this paper.

Acknowledgments

This paper was supported by the National Natural Science Foundation of China (no. 52104015) and the Natural Science Foundation of Shandong Province (no. ZR2021ME001).

References

[1] W. Li, G. Huang, Y. Jing, F. Yu, and H. Ni, "Modeling and mechanism analyzing of casing running with pick-up and release technique," *Journal of Petroleum Science and Engineering*, vol. 172, pp. 538–546, 2019.

[2] C. A. Johancsik, D. B. Friesen, and D. Rapier, "Torque and drag in directional wells-prediction and measurement," *Journal of Petroleum Technology*, vol. 36, no. 6, pp. 987–992, 1984.

[3] M. C. Sheppard, C. Wick, and T. Burgess, "Designing well paths to reduce drag and torque," *SPE Drilling Engineering*, vol. 2, no. 4, pp. 344–350, 1987.

[4] L. Gorokhova, A. Parry, and N. Flamant, "Comparing Soft-String and Stiff-String Methods Used to Compute Casing Centralization," *SPE Drilling & Completion*, vol. 29, no. 1, pp. 106–114, 2014.

[5] B. S. Aadnoy, M. Fazaelizadeh, and G. Hareland, "A 3D analytical model for wellbore friction," *Journal of Canadian Petroleum Technology*, vol. 49, no. 10, pp. 25–36, 2010.

[6] G. Fan, G. Huang, X. Li, and L. Wang, "Calculation model of friction torque for horizontal well string," *Drilling & Production Technology*, vol. 36, no. 5, pp. 22–25, 2013.

[7] D. Gao, "Down-hole tubular mechanics and its applications," University of Petroleum Press, Dongying, China, 2006.

[8] C. Mason and D. C. K. Chen, "Step changes needed to modernise T&D software," in *In SPE/IADC Drilling Conference*, Amsterdam, Netherlands, February, 2007.

[9] H. S. Ho, "General formulation of drillstring under large deformation and its use in BHA analysis," in *In SPE Annual Technical Conference and Exhibition*, New Orleans, Louisiana, USA, October 1986.

[10] R. F. Mitchell and R. Samuel, "How good is the torque/drag model?," *SPE Drilling & Completion*, vol. 24, no. 1, pp. 62–71, 2009.

[11] M. Fan, Y. Jiao, and W. Yu, "Geometric description of borehole centerline in three-dimensional digital simulation of drag in casing running," *Engineering Mechanics*, vol. 22, no. 2, pp. 195–199, 2005.

[12] Q. Liu, J. Jing, and X. Zhu, "Analysis on the form of contact between a drill string and drilled horizontal wellbore and the effects of friction," *Journal of Southwest Petroleum University (Science & Technology Edition)*, vol. 39, no. 5, pp. 163–169, 2017.

[13] R. F. Mitchell, "New concepts for helical buckling," *SPE Drilling Engineering*, vol. 3, no. 3, pp. 303–310, 1988.

[14] J. Bai and Y. Su, "Deviation control theory and practice," Petroleum Industry Press, Beijing, China, 1990.

[15] Y. Chen, F. Liu, X. Zhang, R. Chen, S. Chen, and Z. Zhong, "Numerical simulation of running process of casing string in

horizontal well," *China Petroleum Machinery*, vol. 38, no. 3, pp. 28–30, 2010.

[16] X. Zhu, Y. Gao, S. Liu, and J. Xu, "Feasibility of casing entering curved part in horizontal well," *Oil Field Equipment*, vol. 40, no. 4, pp. 6–8, 2011.

[17] J. Fu, L. Gong, S. Hu, F. Luo, L. Ma, and L. Shang, "Calculation of frictionnal drag of casing running in horizontal well based on ANSYS," *Oil Drilling & Production Technology*, vol. 29, no. 4, pp. 32–35, 2007.

[18] Y. Yu, H. Wang, and C. Miao, "Applications of ANSYS in tripability analysis of casing through horizontal wells," *Oil Field Equipment*, vol. 36, no. 5, pp. 67–69, 2007.

[19] A. Wu, G. Hareland, and M. Fazaelizadeh, "Torque & drag analysis using finite element method," *Modern Applied Science*, vol. 5, no. 6, p. 13, 2011.

[20] Z. Liu, Z. Lian, and L. Wang, "Stress and contact force analysis of whole hole drill string running in directional well," *China Petroleum Machinery.*, vol. 40, no. 6, pp. 13–16, 2012.

[21] V. Tikhonov, V. Khaydar, and N. Albert, "Dynamic model for stiff string torque and drag," *SPE Drilling & Completion*, vol. 29, pp. 279–294, 2014.

[22] X. Qin, D. Gao, and X. Chen, "Effects of initial curvature on coiled tubing buckling behavior and axial load transfer in a horizontal well," *Journal of Petroleum Science and Engineering*, vol. 150, pp. 191–202, 2017.

[23] Y. Shi, Z. Teng, J. Bai et al., "Improved mechanical model of the static push-the-bit rotary steerable bottomhole assembly," *Journal of China University of Petroleum (Edition of Natural Science)*, vol. 42, no. 5, pp. 75–80, 2018.

[24] H. Liu, T. Ma, P. Chen, X. Wang, and X. Wang, "Mechanical behaviors of bottom hole assembly with bent-housing positive displacement motor under rotary drilling," *Arabian Journal for Science and Engineering*, vol. 44, no. 6, pp. 6029–6043, 2019.

[25] X. Liu, *The Geometry of Wellbore Trajectory*, science press, Beijing, China, 2019.

[26] W. Li, X. Li, and G. Huang, "Method of drill string torque and drag of horizontal well based on beam-column theory," *Science Technology and Engineering*, vol. 13, no. 13, pp. 3577–3582, 2013.

[27] W. Gong, "Calculating position of casing centralizer in directional and horizontal well using three-moment of flexure method," *Oil Drilling & Production Technology*, vol. 18, no. 4, pp. 15–24, 1996.

[28] H. Liu and J. Li, "Determining the maximum load in running casing encountered resistance under deep well," *Journal of Southwest Petroleum Institute*, vol. 24, no. 2, pp. 44-45, 2002.

[29] X. Shen and R. Pounds, "Numerical analysis on the 3D mechanical behavior of completion tubing under subsidence loading," in *In International Petroleum Technology Conference*, Kuala Lumpur, Malaysia, December 2014.